Inorganic Chemistry

Article

pubs.acs.org/IC

Thermodynamic Aspects of Aurophilic Hydrogelators

Raquel Gavara,[†,∥] Elisabet Aguiló,[†,∥] Célia Fonseca Guerra,*[,‡] Laura Rodríguez,*[,†] and João Carlos Lima*[,§]

[†]Departament de Química Inorgànica, Universitat de Barcelona, Barcelona, Barcelona 08028, Spain

[‡]Department of Theoretical Chemistry and Amsterdam Center for Multiscale Modeling, VU University, De Boelelaan 1083, 1081 HV Amsterdam, The Netherlands

[§]LAQV-REQUIMTE, Departamento de Química, Faculdade de Ciências e Tecnologia, Universidade Nova de Lisboa, 2829-516 Monte de Caparica, Portugal

Supporting Information

ABSTRACT: The complexes [Au(4-pyridylethynyl)(phosph)] (phosph = PTA (**1**), DAPTA (**2**)) are known to produce supramolecular aggregates and gels in water. We studied the impact of these aggregation processes in the absorption spectra, ^{1}H NMR (at different temperatures and concentrations), and DLS and estimated the equilibrium constant for a single step aggregation of the molecule (K = 26760 and 2590 M^{-1} for **1** and **2**, respectively, at 25 °C). We present spectroscopic evidence for the presence of Au···Au contacts in the aggregates: the recorded changes on ^{1}H NMR and the appearance of new absorption bands assigned to ($\sigma^*_{Au\cdots Au}-\pi^*$) have been attributed to the short (Au···Au) average distances in the aggregates. Relativistic density functional theory computations support the existence of short Au···Au distances and reveal charge-transfer in the aurophilic interactions. The free energy for a single step aggregation was calculated from the experimental data, and the value obtained ($\Delta G \sim -20$ kJ/mol) is in good agreement with the expected values in the order of the energies found for hydrogen bonds. The DFT computations confirm the experimental findings that aggregation of monomer **1** is stronger than the aggregation of monomer **2** and the existence of aurophilic interactions.

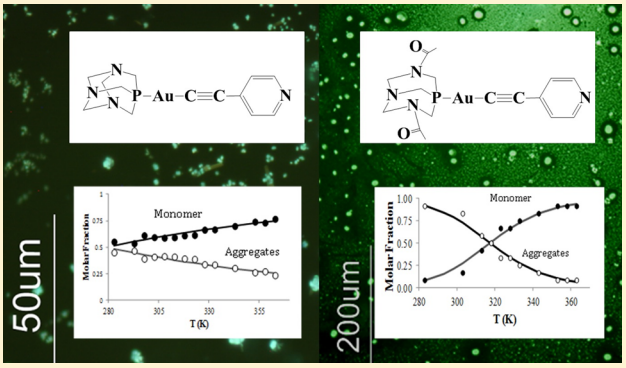

INTRODUCTION

Gold(I) complexes are known to exhibit interesting emissive properties that usually are modulated by the presence of aurophilic (Au···Au) interactions.[1−4] These interactions are a consequence of the strong relativistic effects displayed by gold atoms, and their energy can range from 20 to 50 kJ/mol[5,6] which is comparable to that of strong hydrogen bonds.[7] Recently, they have been observed to be involved in the formation of a specific type of large supramolecular structures leading to gel formation in water, which includes these compounds in the class of low molecular weight hydrometallogelators.[8] The presence of metal ions in the chemical structure gives rise to additional properties and exciting potential applications of hydrometallogels which include catalytic activity,[9,10] bioimaging,[11,12] controlled release of drugs,[13] among others. Metallophilic interactions, in some particular metal complexes, like Au(I) derivatives, play a key role for the primary aggregation and may lead to increased gelating ability of small molecules and rich photophysical properties induced by gelation.[14−16] Au(I) has shown to be very effective in potentiating the gelation process, and it should be highlighted that interactions involving Au(I) atoms have been reported to be present in most of the organo- and hydrogold metallogelators reported in the literature.[8] For example Odriozola, Dupin, and co-workers[17] have produced gels very recently by the addition of Au(I) ions to thiol therminated PEG. A 3D network has been observed for these authors to be formed where the thiolated ends are "'sewed'" together via Au−S interactions and further aligned in a zigzag conformation, through aurophilic interactions.

Although aurophilic bonding has been extensively observed in the solid state, with through X-ray diffraction, the number of cases where this kind of interaction has been observed in solution is still scarce. Several techniques and methods have been employed to attribute the occurrence of intra- and intermolecular aurophilicity in solution, including EXAFS,[18−20] X-ray diffraction in solution,[21] cyclic voltammetry,[22] mass spectrometry,[23,24] NMR,[23−27] UV−vis absorption spectroscopy,[25,27−31] and emission studies, regarding concentration dependent emission,[32] luminescence bands assigned to Au···Au bonded excimers and exciplexes,[33] occurrence of emission bands characteristic of aurophilic contacts (MC or MMLCT transition),[34] and effect on the radiative and nonradiative rate constants.[35]

Received: January 7, 2015
Published: May 20, 2015

DOI: 10.1021/acs.inorgchem.5b00025
Inorg. Chem. 2015, 54, 5195−5203

Chart 1

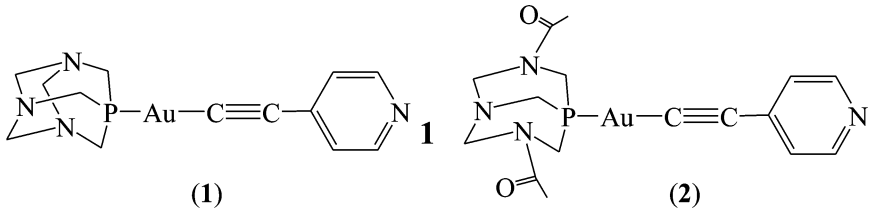

(1) (2)

Recently we reported on the autoassociation properties of [Au(4-pyridylethynyl)(phosph)] (phosph = PTA (1,3,5-triaza-7-phosphaadamantane), **1**[36] and DAPTA (3,7-diacetyl-1,3,7-triaza-5-phosphabicyclo[3.3.1]nonane), **2**[37]) complexes (Chart 1) in water. These compounds are able to aggregate in this solvent up to the formation of very long fibers that originate, as a last resort, a gel structuration. The driving forces for the aggregation process can be both intermolecular $\pi-\pi$ stacking between (4-pyridyl)ethynyl chromophores and aurophilic interactions between gold(I) atoms of neighbor molecules.

In this work, we study the impact of the aggregation in the absorption bands and ^{1}H NMR spectra recorded at different temperatures and concentrations in order to evaluate the participation of Au···Au interactions in the supramolecular assemblies of the molecules leading to the formation of gels.

The design of gelators with novel structures remains a challenging task.[8−16,38] In this sense, the organization introduced by the Au···Au intermolecular interactions in aurophilic gels adds one more valuable piece to the rational design toolbox. The wide range of potential applications of such structures justifies the effort on the study and analysis of the main factors that could govern the establishment of intermolecular interactions in the gels formed by the additional contribution of gold metallophilic interactions. In particular, the understanding of the driving force leading to aggregation should be a key point for the design and improvement of new hydrometallogelator molecules.

RESULTS AND DISCUSSION

UV−vis Absorption in Water. The absorption spectrum of an aqueous solution of **1** at ca. 2.5×10^{-4} M, 3 days old, can be seen in Figure 1. The solution, which was clear immediately after preparation, shows increasing turbidity with time and the appearance of a broad band with a maximum around 375 nm apart from the vibronically well resolved band centered at 275 nm corresponding to the chromophoric unit, 4-ethynylpyridine.[36] After filtering the solution with a 0.45 μm filter, the broad band disappears, indicating that it corresponds to aggregates bigger than the pore size of the filter.

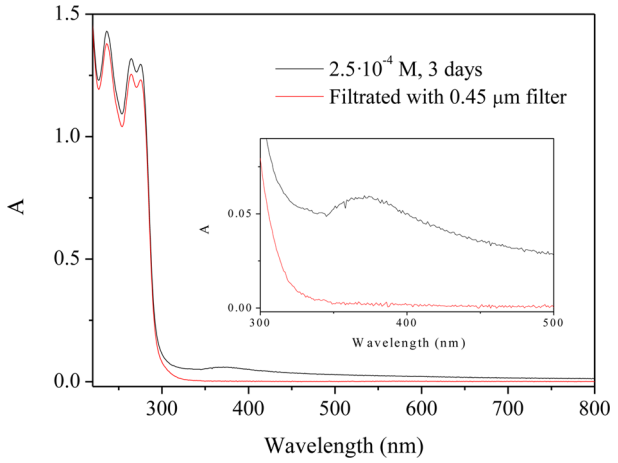

Figure 1. Absorption spectra of an aqueous solution of **1** (2.5×10^{-4} M); black line − 3 days old solution; red line − same solution after filtration with a 0.45 μm filter.

Similar experiments carried out at lower concentrations indicate also the formation of aggregates due to similar changes on the absorption spectra (Figure S1). At the same time, the emission spectra show the decrease of the monomer emission band together with the formation of a new lower energy band (aggregates' emission). Excitation spectra collected at the emission maxima indicate the increase weight of the aggregates in the observed emission (Figure S2).

The same general features are also observed for a 1.5×10^{-4} M aged aqueous solution of **2** (Figure S3). The absorption decreases due to some precipitation of fibers but also due to the appearance, with time, of a broad absorption band with local maxima around 316 and 340 nm.

In both cases the aggregation produces new bands at wavelengths above 300 nm which agree with the presence of ($\sigma^*_{Au\cdots Au}-\pi^*$) transitions[35−37] in the aggregates due to (Au···Au) aurophilic contacts.

In the filtrates and in fresh solutions these bands are strongly reduced at the concentrations used in UV/vis spectroscopy. However, DLS measurements still show the presence of smaller aggregates in solution (see below).

Dynamic Light Scattering Measurements in Water of Fresh Solutions. Dynamic Light Scattering experiments were carried out with freshly prepared solutions in order to analyze the presence of aggregates at low concentrations in these conditions and not only in aged solutions. Interestingly, the presence of agglomerates with ca. 100 nm (for **1**, 2×10^{-5} M) and 150 nm (for **2**, 1.5×10^{-4} M) size were detected being indicative that the complexes aggregate in solution also at very low concentrations (see Figure 2). The difference in concentration for the compounds is because **1** aggregates in water up to a much lower concentration than **2**. The higher solubility of **2** precludes the formation of analogous aggregates at the same concentrations range.

Fluorescence and Optical Microscopy additionally support the hypothesis that the initial aggregation steps lead to the formation of spherical aggregates which evolve with time rendering the formation of larger spherical aggregates (Figures 3 and S4) as precursors of fibers formed at a later stage.[36,37]

NMR vs Concentration in Water. ^{1}H NMR spectra of aqueous solutions of **1** at different concentrations display two groups of pyridyl protons at $\delta(H_\alpha)$ 8.53 and 8.44 ppm and $\delta(H_\beta)$ 7.55 and 7.39 ppm. The first group (H_α 8.53 ppm and H_β 7.55 ppm) grows in intensity with respect to the second when increasing concentration (Figure 4) and is thus assigned to the aggregates that seem to be in slow exchange with the

DOI: 10.1021/acs.inorgchem.5b00025
Inorg. Chem. 2015, 54, 5195−5203

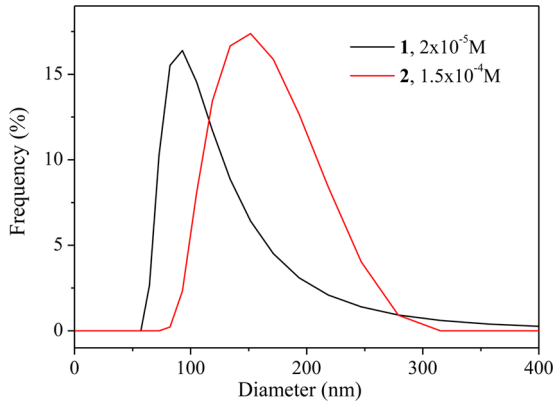

Figure 2. DLS size distributions for fresh aqueous solutions of **1** (2×10^{-5} M) and **2** (1.5×10^{-4} M).

monomers. Molar fractions can be therefore straightforward retrieved from integration of the NMR signals (see below).

On the other hand, ^{1}H NMR spectra of aqueous solutions of **2** at several concentrations display only one group of pyridyl protons at lower concentrations which are observed to shift upfield upon increasing the concentration (Figure 5). In this case, the early aggregates seem to be in fast exchange with the monomers, and molar fractions must be retrieved from the weighted average of the extrapolated monomer and aggregate shifts (see below). Moreover, it is observed a splitting of the signals in two groups at the highest concentrations, indicative of different environments for H_α and H_β protons. The different set of signals that appears at higher concentrations seems to be in slow exchange with the other species.

The molar fractions of monomer and aggregate were obtained from the chemical shifts of the more intense signals. Those signals present a significant upfield shift with aggregation, and, more importantly, they can be followed continuously from the lowest to the highest concentration. The molar fraction of the new population of aggregates in slow exchange can also be obtained from the integration of the peaks, but we cannot know with which species this second equilibrium at higher concentration is related (monomers or early stage aggregates).

The ^{1}H NMR spectra show important differences in the aggregation behavior of **1** and **2**: a) compared to ^{1}H NMR time scale the monomer/aggregate exchange in **1** is very slow, while it is fast for **2**; compound **2** presents a significant upfield shift of the pyridyl protons with aggregation, while aggregation of **1** produces a downfield shift of the same protons. The differences in behavior might be related with the establishment of weak intermolecular interactions between the carbonyl groups at the phosphines and the hydrogens of the pyridyl unit (see the Computational Studies section).

^{31}P NMR spectra recorded at the same concentration range are in agreement with the aggregation process. It could be seen that the chemical shift of **2** becomes slightly broader and ca. 3 ppm upfield shifted when increasing concentration due to the establishment of interactions with neighbor molecules (Figure S5). A similar experiment was not possible to carry out with **1** due to the lower solubility of this complex in water.

NMR vs Temperature in Water. ^{1}H NMR experiments were also carried out for both complexes at the same concentration (ca. 1×10^{-3} M) at different temperatures.

In the case of **1**, the increase in temperature gives rise to a decrease in the less shielded H_α and H_β pyridyl protons, previously assigned to aggregates (Figure 6 left), i.e., that the increase in temperature shifts the equilibrium toward the monomers.

In the case of **2**, the increase in temperature induces a downfield shift, both in ^{1}H- and ^{31}P NMR, also compatible with the shift of equilibrium toward the monomer (Figure 7 and S6). Additionally, an ca. 0.03−0.1 ppm upfield shift of the phosphine protons is also detected for this complex (Figure S7). These data support the involvement of both ligands (pyridine and phosphine) in the aggregation process for **2**. This fact could be indicative of weak intermolecular interactions involving the acetyl unit, which are absent in **1**, in agreement with the lack of significant shift of the same protons with temperature (Figure S7). Hence, the additional involvement of the phosphines (mainly related to the additional establishment of hydrogen bonds) could be responsible for the formation of higher entangled fibers in **2**[37] with respect to **1**.[36] The opposing shifts of both groups of protons (down and upfield, for pyridine and phosphine protons respectively) are consistent with a head to tail disposition of some molecules in the supramolecular assemblies and in agreement with NOE interactions previously reported for **1**[36] and X-ray crystal diffraction of other similar complexes reported recently in the literature.[39,40]

The recorded variations of peak intensities and chemical shift in the case of **1** and **2**, respectively, both follow a sigmoidal behavior. This is common for an aggregation process that follows an isodesmic model,[41] with two limiting states (monomers and aggregates of order *n*, see below) linked by a number of intermediate aggregated states. This model can be applied to ^{1}H NMR shifts vs temperature and concentration

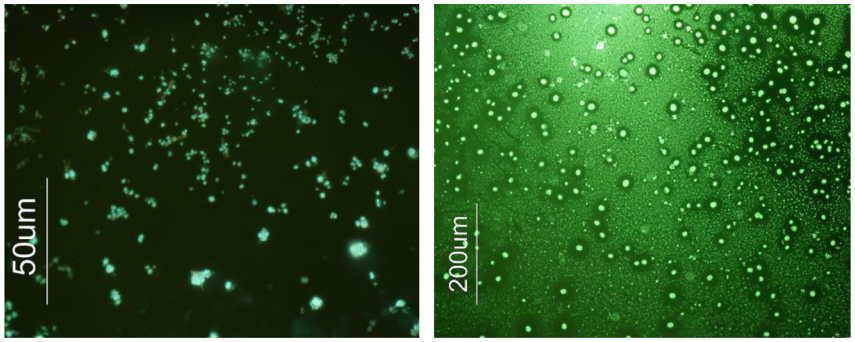

Figure 3. Fluorescence microscopy images of dried samples of **1** (left) and **2** (right) after 1 h of solubilization in water and immediately analyzed after evaporation to dryness. Excitation filter: 395−440 nm.

DOI: 10.1021/acs.inorgchem.5b00025
Inorg. Chem. 2015, 54, 5195−5203

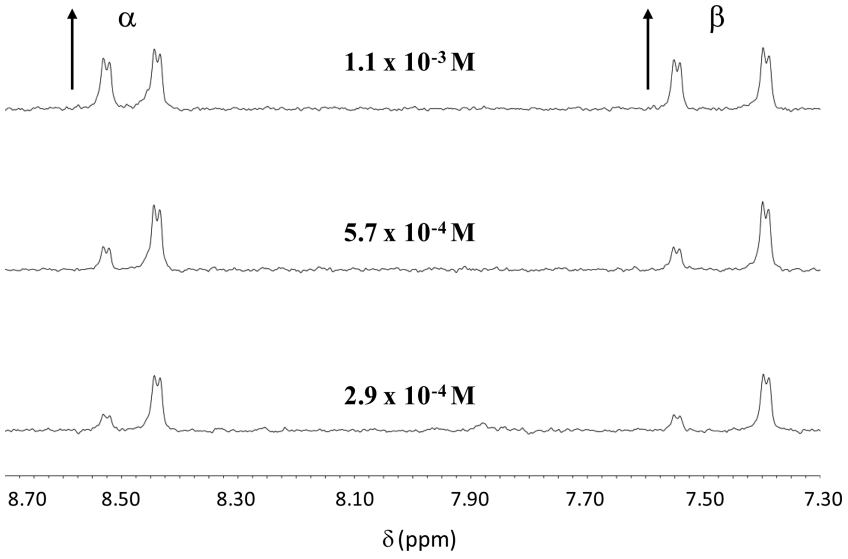

Figure 4. ^{1}H NMR spectra of aqueous solutions of **1** at different concentrations and 288 K.

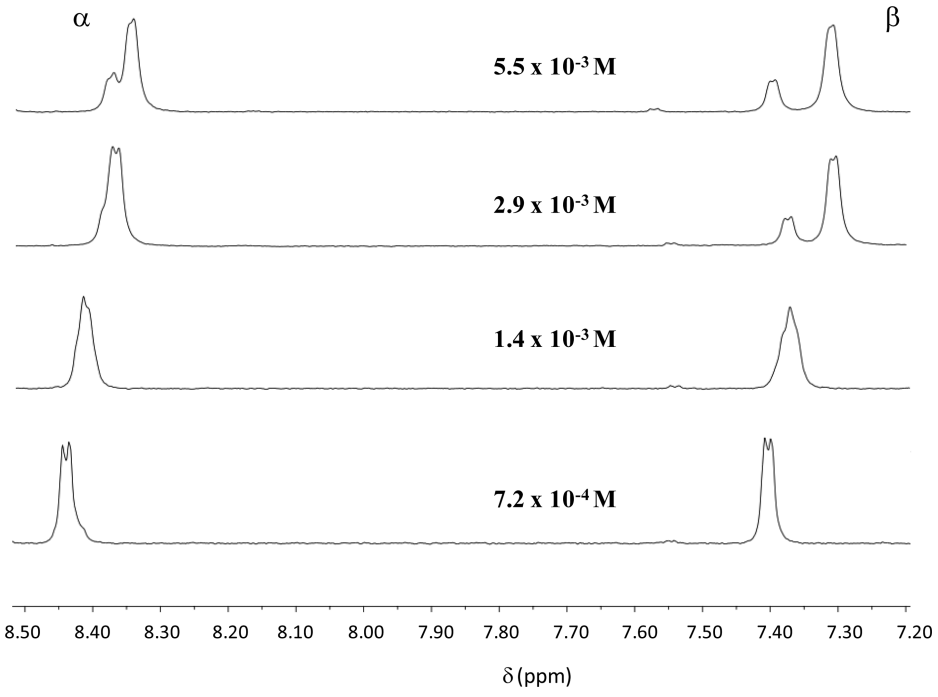

Figure 5. ^{1}H NMR spectra of aqueous solutions of **2** at different concentrations and 288 K.

experiments and has been recently applied for supramolecular naphthalenediimide nanotube formation.[42,43]

In the case of **1**, the molar fractions of monomer and aggregate states were obtained from the integration of the respective NMR peaks. In the case of **2**, it was necessary to extrapolate the chemical shifts of monomer and aggregate (δ_{mon} = 8.48 ppm, δ_{agreg} = 8.36 ppm, respectively) to obtain the experimental molar fractions of monomer and aggregates from the chemical shifts $\{x_{mon} = (\delta_{obs}-\delta_{agreg})/(\delta_{mon}-\delta_{agreg})\}$.

Isodesmic Model. In order to obtain thermodynamic information from the aggregation process we must take into account that different types of aggregates will be present simultaneously in solution, even if some of them will show similar spectral features. The aggregation steps are exemplified in eqs 1−3

$$M + M \rightleftarrows M_2 \quad c_2 = K_2 c_1^2 \tag{1}$$

$$M_2 + M \rightleftarrows M_3 \quad c_3 = K_3 c_2 c_1 = K_2 K_3 c_1^3 \tag{2}$$

$$M_{n-1} + M \rightleftarrows M_n \quad c_n = K_n c_{n-1} c_1 = K_2 K_3 \ldots K_n c_1^n \tag{3}$$

where c_n is the concentration of the aggregate n (n = 1: monomer, n = 2: dimer, etc.), and K_n is the aggregation constant of the corresponding process.

In the isodesmic assumption all the K_n constants are considered equal, i.e., $K_n = K$, which is reasonable to be applied in our case where the consecutive aggregation steps are ruled by the same thermodynamic driving force. In this case, the concentration $c_n = K^{n-1} c_1^n$ and the total concentration c_0 can be presented by the sum in eq 4

DOI: 10.1021/acs.inorgchem.5b00025
Inorg. Chem. 2015, 54, 5195−5203

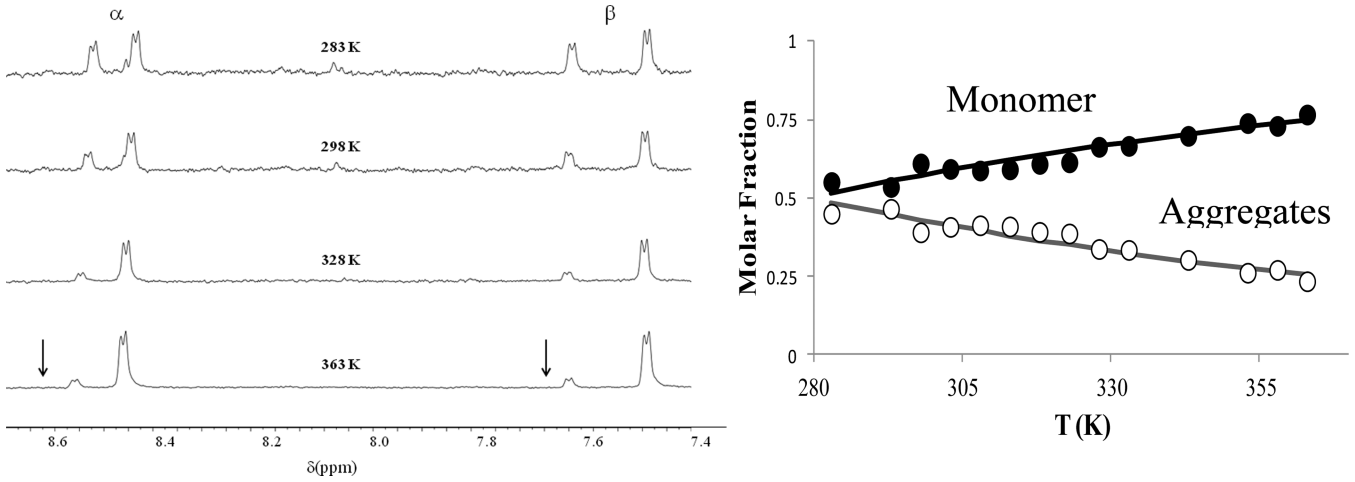

Figure 6. ^{1}H NMR spectra of 1×10^{-3} M aqueous solution of **1** at different temperatures (left); closed circles − molar fractions of the monomer; open circles − molar fraction of aggregates ($x_{agg} = 1 - x_{mon}$); lines − fitting of the molar fractions with isodesmic model (see below) adapted to account the temperature effect on the constants (right).

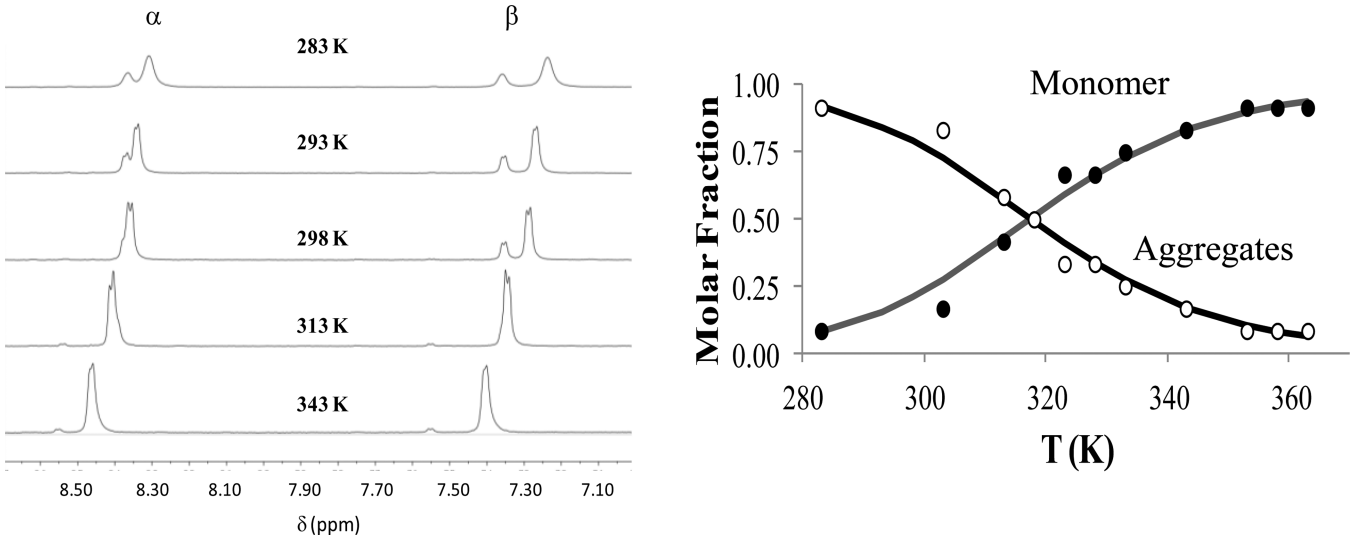

Figure 7. ^{1}H NMR spectra of 1×10^{-3} M aqueous solution of **2** at different temperatures (left); closed circles − molar fractions of the monomer; open circles − molar fraction of aggregates ($x_{agg} = 1 - x_{mon}$); lines − fitting of the molar fractions with isodesmic model (see below) adapted to account the temperature effect on the constants (right).

$$c_0 = c_1 + 2Kc_1^2 + 3K^2c_1^3 + \ldots + nK^{n-1}c_1^n \quad (4)$$

which yields eq 5 upon division by c_1.

$$\frac{c_0}{c_1} = 1 + 2Kc_1 + 3K^2c_1^2 + \ldots + nK^{n-1}c_1^{n-1} \quad (5)$$

The right side of eq 8 is a convergent series if $0 < Kc_1 < 1$, in which case

$$1 + 2(Kc_1) + 3(Kc_1)^2 + \ldots + n(Kc_1)^{n-1} = \frac{1}{(1 - Kc_1)^2} \quad (6)$$

yielding a simple quadratic equation that relates the concentration of monomer, c_1, the total concentration, c_0, and the stepwise aggregation constant, K.

$$c_0 = \frac{c_1}{(1 - c_1K)^2} \quad (7)$$

The molar fractions of monomer, x_1, and aggregates, x_n, are thus given by eqs 8 and 9.

$$x_1 = \frac{c_1}{c_0} = \frac{1 + 2Kc_0 - \sqrt{1 + 4Kc_0}}{2K^2c_0^2} \quad (8)$$

$$x_n = 1 - x_1 = 1 - \frac{1 + 2Kc_0 - \sqrt{1 + 4Kc_0}}{2K^2c_0^2} \quad (9)$$

In both cases, the equilibrium constant will change with temperature according to eq 10

$$K = e^{-(\Delta G/RT)} \quad (10)$$

where ΔG is the free energy change during the aggregation process. However, ΔG is also temperature dependent, and a more adequate expression to fit is eq 11 provided that ΔH and ΔS are constant in the temperature range used, which is a good approximation if the temperature range is small.

$$K = e^{-((\Delta H/RT)+(\Delta S/R))} \quad (11)$$

DOI: 10.1021/acs.inorgchem.5b00025
Inorg. Chem. 2015, 54, 5195−5203

The values obtained from the fittings shown above are summarized in Table 1.

Table 1. Enthalpy, Entropy, Free Energy at 298 K, and Aggregation Constant at 298 K for Aqueous Solutions of Compounds 1 and 2 at 1×10^{-3} M

compound	ΔH/kJ·mol^{-1}	ΔS/J mol^{-1} K^{-1}	ΔG^{298}/kJ mol^{-1}	K^{298}
1	-19 ± 7^a	21 ± 9	-25 ± 1	26760
2	-60 ± 0.5	-136 ± 2	-19 ± 0.5	2590

[a]The error in ΔH and ΔS determinations in **1** arises from the low solubility of the compound; this error was estimated from the differences in molar fractions determined against the total area of the pyridyl protons and against the area of an internal reference.

In both cases a negative enthalpy contributes for the aggregation, which can arise not only from multiple contributions such as the stabilizing interaction between monomers (H-bonds, $\pi\pi$-stacking, Au···Au interactions) but also from changes in the solvation energy of monomers and aggregates. The more hydrophilic complex **2** has a negative change on entropy upon aggregation, while the more hydrophobic monomer **1** presents a positive change in entropy, probably associated with the release of water molecules during aggregation. These opposite effects make the free energy change in both systems very comparable, even if the enthalpic contributions are very different.

Computational Studies. We have computationally analyzed the formation of dimers and tetramers from **1** to support our experimental findings with the Amsterdam Density Functional program at the ZORA-BLYP-D3(BJ)/TZ2P level of theory.[44,45] For monomer **2**, we have considered only the formation of dimers because the tetramers were computationally too demanding. The smallest unity for the formation of the gels is the dimer. There are different possibilities of dimerization for monomer **1** (depicted in Figure 8) which take into account the possible weak van der Waals interactions. For the dimerization of monomer **2**, we considered the most likely structure, which was based on the lowest-energy conformation of the dimer of **1**.

For the possible dimers presented in Figure 8, the dimerization energies, Au···Au distances, and the ^{1}H NMR spectra for the pyridine ligands of **1** are given in Table 2. Dimer III did not converge to any minimum, so it will not be considered. The most likely dimers are II and IV, because they have the largest dimerization energy (−68.5 kJ/mol and −78.0 kJ/mol, respectively) and their ^{1}H NMR spectra follow the experimental trend. Upon dimerization, the $\delta(H_\alpha)$ and $\delta(H_\beta)$ of pyridines shift downfield as can be seen in Figure 4, and this downfield shift is found computationally for dimers II and IV and not for dimer I (see Table 2). For example, the computed value of $\delta(H_\alpha)$ is 8.80 ppm in the monomer and 8.87 in dimer II, and $\delta(H_\beta)$ is 7.57 ppm in the monomer and 7.70 ppm in the dimer.

We have extended our computations to the formation of the tetramers, which are formed by bringing two dimers together. The bond energy between two dimers in the tetramers is given in Table 2. These computations reinforce our previous computational findings that there is a close Au···Au contact in the gels. There is a larger gain in energy, −112.5 kJ/mol by forming IV−IV from two dimers IV than with the formation of I−I or II−II. We have considered different options by removing symmetric constraints (C_1), but the C_2 symmetric tetramer IV−IV resulted in the lowest bonding energy. Computational experiments showed that the monomers can rotate quite easily around the axis formed by the gold atoms. The structures of the tetramers were computationally too demanding to do vibrational analysis. The computed Gibbs energy of dimer IV −34.3 kJ/mol is also closest to the experimental value of 25 ± 1 kJ/mol. Still we must be aware of the fact that the computations are only a first approximation to the simulation of the aggregation in the solvent between larger amounts of monomers.

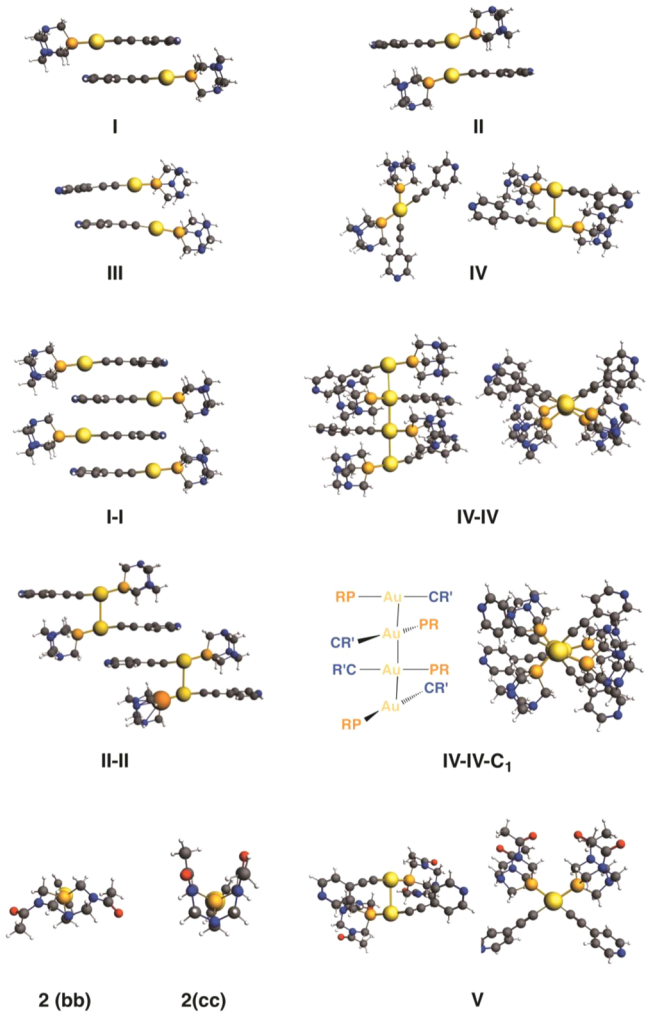

Figure 8. Possible dimers and tetramers in gel formation of **1** and **2** (ZORA-BLYP-D3(BJ)/TZ2P with COSMO).

For monomer **2**, there are two possibilities for the DAPTA ligand: the chair−chair (cc) and the boat−boat (bb) conformation (see Figure 8). The cc conformation is 39.3 kJ/mol lower in energy than the bb conformation. No local minimum could be found for the chair−boat conformation. For the dimerization of monomer **2** the cc conformation was used in the computations and only structure V (Figure 8) equivalent to dimer IV was considered, because a dimerization as in II is not likely to occur due to the bulkier phosphine ligand in monomer **2**. The computed Gibbs energy for dimer V amounts to −10.2 kJ/mol and is smaller than for dimer IV. This order of strength is in line with the experiments.

The computed ^{1}H NMR chemical shifts for the pyridyl rings of monomer **2** are 8.77 and 7.54 ppm. The NMR computations of dimer V do not capture the whole experiment as they do not

DOI: 10.1021/acs.inorgchem.5b00025
Inorg. Chem. 2015, 54, 5195−5203

Table 2. Bond Energies and Gibbs Free Energies (kJ/mol), Au···Au Distances (Å), and ^{1}H NMR Spectra (ppm)[a]

	symmetry	ΔE[b]	ΔG	Au···Au (Å)	$\delta(H_\alpha)$	$\delta(H_\beta)$
Monomer 1					8.73	7.51
Dimers of 1						
I	C_{2h}	−65.0	−11.3	7.32	8.82	7.48
II	C_{2h}	−68.5	−7.5	3.32	8.79	7.65
III	C_1					
IV	C_2	−78.0	−34.3	3.15	8.80/8.80	7.63/7.68
Tetramers of 1						
I−I	C_{2h}	−63.0		7.57		
II−II	C_{2h}	−44.9		8.79		
IV−IV	C_2	−112.5		3.02		
IV−IV−C_1	C_1	−101.1		3.05		
Monomer 2	C_1				8.77/8.76	7.54/7.56
Dimer of 2						
V	C_2	−63.7	−10.2	3.15	8.82/8.81	7.69/7.58

[a]Bond energies and structures computed at the ZORA-BLYP-D3(BJ)/TZ2P and ^{1}H NMR chemical shifts computed at the ZORA-SAOP/TZ2P with COSMO (water). [b]Bond energy, ΔE, is defined as for the dimers as $E_{dimer} - 2*E_{monomer}$ and for the tetramer as $E_{tetramer} - 2*E_{dimer}$

reproduce the experimental values. Other factors in the aggregation process (e.g. $\pi-\pi$ stacking or hydrogen bonding) could also be influencing the NMR spectrum, but the computations show that the formation of the aurophilic bond in dimer IV and V is responsible for a deshielding of the pyridyl protons as for monomer **1** and monomer **2** a downfield shift is observed in the computations. The observed upfield shift for monomer **2** in the experiments due to the formation of aggregates can be explained with the structural differences between monomers **1** and **2**. Monomer **2** has a carbonyl group on the phosphine ligand which can form hydrogen bonds with the C−H bonds of the pyridines. Hydrogen bonds include a weak donor−acceptor interaction which causes electronic density to flow from the lone pair of the proton acceptor (in this case the oxygen atom of the carbonyl group) to the antibonding orbital of the C−H bond.[47,48] It was not possible to compute these very weak hydrogen bonds within dimer V. (Also dimerization of monomer **2** via hydrogen bonds only, that is without Au···Au interaction, is computationally not accessible as the system will try to form the more favorable aurophilic interaction.) The computational evidence for the formation of the hydrogen bonds between the lone pair of the oxygen in monomer **2** and the C−H groups of pyridine can be rationalized with the energy levels of molecular orbitals. In the aggregates of monomer **1**, there can only be hydrogen bonding between the water and pyridine ligands. In the aggregates of monomer **2**, there is a competition between the lone pairs of the oxygen atoms of water and the carbonyl group to form hydrogen bonds. These hydrogen bonds are stronger for the carbonyl group as the lone pair of the carbonyl group is higher in energy (at −6.2 eV) than of water (at −7.5 eV, see Figure S8a). The carbonyl group has a smaller energy gap between the lone pair of oxygen and the accepting antibonding orbital of the C−H group.

The last point addressed is the nature of the aurophilic interactions in the gels. From theoretical work[46] it is known that relativistic effects and dispersion interactions are responsible for the Au···Au bonding[5] with a small covalent contribution. Kohn−Sham MO analysis[44] of the aurophilic interactions upon dimerization of **1** shows indeed charge-transfer from occupied orbitals of one moiety to the unoccupied orbitals of the other monomer and back from the latter monomer to the former. For the formation of the dimer, we find that the HOMO-6 (Figure S8b) of one monomer **1** donates (0.04 electrons) into the LUMO of the other monomer **1** (0.03 electrons). This also occurs in the other way around: the former monomer accepts 0.03 electrons in the LUMO and the latter donates 0.04 electrons from the HOMO-6. The donation and acceptation are not canceling each other exactly, because there is also polarization (mixing of occupied and unoccupied orbitals) within one monomer due to the presence of the other monomer.

When we remove the virtuals (unoccupied) from one of the monomers, this monomer cannot accept charge nor can there be polarization on this monomer due to the presence of the other one. Computations with one monomer without virtuals show that this monomer still loses 0.02 electrons to the other monomer, which proves the existence of the covalent component in the Au···Au interactions. The strength and the charge-transfer interactions in the aurophilic interactions are of the same order of magnitude as in hydrogen bonds.[47]

CONCLUSIONS

The analysis of spectroscopic data based on absorption and ^{1}H NMR data at different concentrations and temperature was used to get information about the thermodynamic aspects of the aggregation of the [Au(4-pyridylethynyl)(phosph)] (phosph = PTA, DAPTA) complexes which are able to act as gelators in water.

From the absorption data it is possible to infer that aggregation gives rise to the presence of a long-wavelength tail whose origin could be related with a ($\sigma^*_{Au\cdots Au}-\pi^*$) transition and the presence of aurophilic Au···Au contacts (~3.5 Å).

This broad band is observed to increase in old samples where the aggregates are more favored (long fibers). The aggregation with short Au···Au distances is confirmed by computational DFT studies.

^{1}H NMR spectra recorded at different temperatures and concentrations indicate a different interconversion between monomer and aggregate environment that is faster in the case of **2** than for **1**. The data retrieved from these experiments was fitted with the isodesmic model of aggregation, and the equilibrium constant at 25 °C for a single aggregation step was obtained. This equilibrium constant corresponds to a free energy change of ca. −20 kJ/mol, but the weight of enthalpic

DOI: 10.1021/acs.inorgchem.5b00025
Inorg. Chem. 2015, 54, 5195−5203

and enthropic contributions is quite different in both complexes.

Relativistic density functional theory computations were then used to analyze the Au···Au interaction contribution to the overall free energy. The DFT computed Gibbs energy for dimers of **2** is predicted to be smaller than for dimers of **1**. The DFT order of strength is in good agreement with the free energies calculated from ^{1}H NMR data, which support the existence of short Au···Au distances and reveal charge-transfer (covalent component) in the aurophilic interactions.

EXPERIMENTAL SECTION

General Procedures. Synthesis of [Au(4-pyridylethynyl)(PTA)] and [Au(4-pyridylethynyl)(DAPTA)] complexes were reported elsewhere.[36,37]

Physical Measurements. Solutions were prepared with Millipore water and spectroscopic grade solvents. Absorption spectra were acquired on a Varian Cary 100 Bio spectrophotometer. In heating experiments, the temperature of the cell was regulated to ±0.1 °C by a circulating water bath.

^{1}H NMR (δ(TMS) = 0.0 ppm) and ^{31}P{^{1}H}-NMR (δ(85% H_3PO_4) = 0.0 ppm) spectra were obtained on a Varian Unity 400 and Bruker DMX 500 MHz at the Centres Científics i Tecnològics de la Universitat de Barcelona (CCiTUB). Variable temperature NMR experiments were carried out by using 3-(trimethylsilyl)-2,2′,3,3′-tetradeuteropropionic acid as external reference.

Dynamic light scattering measurements were carried out on a SZ-100 Nanoparticle Analyzer (HORIBA) instrument operating at 22 °C.

Fluorescence microscopy was recorded on an Axioplan 2ie Zeiss imaging microscope equipped with a NikonDXM1200F digital camera. Excitation light for fluorescence imaging was selected using filters in the range 395−440 nm. The samples were freshly prepared in ca. 1×10^{-4} M concentration. A few drops were deposited in a microscope support, and the solvent evaporated until dryness.

Computational Details. All calculations have been performed using the Amsterdam Density Functional (ADF) program[44,45] using relativistic density functional theory at the ZORA-BLYP-D3(BJ)/TZ2P for geometry optimization and energies and at SAOP/QZ4P//BLYP-D3(BJ)/TZ2P for ^{1}H NMR chemical shifts relative to TMS.[49−51] Solvation in water is simulated using the conductor-like screening model (COSMO).[52−55] The stationary points of the monomer and dimers were verified to be minima on the potential energy surface (PES) through vibrational analysis.

ASSOCIATED CONTENT

Supporting Information

Absorption spectra changes of an aqueous solution of **1** (1×10^{-4} M) with time (Figure S1); Excitation spectra changes of an aqueous solution of **1** (1×10^{-4} M) with time (λ_{em} = 405 nm), left; Emission spectra of an aqueous solution of **1** (1×10^{-4} M) with time (right) (Figure S2); Absorption spectra of an aqueous solution of **2** (1.5×10^{-4} M); black line − freshly prepared; red line − same solution after 1 month (Figure S3); Optical microscopy images of a dried sample of **2** (Figure S4); ^{31}P NMR spectra of aqueous solution of **2** at different concentrations and 298 K (Figure S5); ^{31}P NMR spectra of aqueous solution of **2** at different temperatures (Figure S6); N-CH_2-P (phosphine) chemical shifts recorded for **2** (A) and for **1** (B) at different temperatures (Figure S7); (a) Lone pair of the oxygen atom of the carbonyl group of monomer **2** (left) and the lone pair of water (right). (b) The HOMO-6 and the LUMO of the monomer **1** (Figure S8); Cartesian coordinates of monomers of **1**, dimers of **1**, and tetramers of **1** in water (Table S1); Cartesian coordinates of monomers of **2** and dimers of **2** in water (Table S2). The Supporting Information is available free of charge on the ACS Publications website at DOI: 10.1021/acs.inorgchem.5b00025.

AUTHOR INFORMATION

Corresponding Authors

*E-mail: c.fonsecaguerra@vu.nl.

*Phone: 34 934039130. Fax: 34 934907725. E-mail: laura.rodriguez@qi.ub.es.

*Phone:351 212948300 (ext. 10923). Fax: 351 212948550. E-mail: lima@fct.unl.pt.

Author Contributions

‖Both authors contributed equally to this work.

Notes

The authors declare no competing financial interest.

ACKNOWLEDGMENTS

The support and sponsorship provided by COST Actions CM1005 and CM1105 are acknowledged. The authors are also grateful to the Ministerio de Ciencia e Innovación of Spain (Project CTQ2012-31335) and Fundação para a Ciência e Tecnologia of Portugal (PTDC/QUI-QUI/112597/2009; PEst-C/EQB/LA0006/2011). This research was supported by a Marie Curie Intra European Fellowship within the seventh European Community Framework Programme (R.G.). We would like to thank Denisa Kubániová and Francesco Zaccaria for the helpful contributions.

REFERENCES

(1) Schmidbaur, H.; Schier, A. *Chem. Soc. Rev.* **2012**, *41*, 370.
(2) He, X. M.; Yam, V. W. W. *Coord. Chem. Rev.* **2011**, *255*, 2111.
(3) Lima, J. C.; Rodríguez, L. *Chem. Soc. Rev.* **2011**, *40*, 5442.
(4) Yam, V. W. W.; Wong, K. M. C. *Chem. Commun.* **2011**, *47*, 11579.
(5) Pyykkö, P. *Chem. Soc. Rev.* **2008**, *37*, 1967.
(6) Schmidbaur, H.; Graf, W.; Müller, G. *Angew. Chem., Int. Ed.* **1988**, *47*, 417.
(7) Steiner, T. *Angew. Chem., Int. Ed.* **2002**, *41*, 48.
(8) Lima, J. C.; Rodríguez, L. *Inorganics* **2015**, *3*, 1.
(9) Buhler, G.; Feiters, M. C.; Nolte, R. J. M.; Dotz, K. H. *Angew. Chem., Int. Ed.* **2003**, *42*, 2494.
(10) Díaz, D. D.; Kühbeck, D.; Koopmans, R. J. *Chem. Soc. Rev.* **2011**, *40*, 427.
(11) Bull, S. R.; Guler, M. O.; Bras, R. E.; Meade, T. J.; Stupp, S. I. *Nano Lett.* **2005**, *5*, 1.
(12) Mauro, M.; Aliprandi, A.; Septiadi, D.; Kehra, N. S.; de Cola, L. *Chem. Soc. Rev.* **2014**, *43*, 4144.
(13) Saha, S.; Bachl, J.; Kundu, T.; Díaz Díaz, D.; Banerjee, R. *Chem. Commun.* **2014**, *50*, 7032.
(14) Tam, A. Y.-Y.; Yam, V. W.-W. *Chem. Soc. Rev.* **2013**, *42*, 1540.
(15) Strassert, C. A.; Chien, C.-H.; Galvez Lopez, M. D.; Kourkoulos, D.; Hertel, D.; Meerholz, K.; de Cola, L. *Angew. Chem., Int. Ed.* **2011**, *50*, 946.
(16) Kishimura, A.; Yamashita, T.; Aida, T. *J. Am. Chem. Soc.* **2005**, *127*, 179.
(17) Casuso, P.; Pérez-San Vicente, A.; Iribar, H.; Gutiérrez-Rivera, A.; Izeta, A.; Loinaz, I.; Cabañero, G.; Grande, H.-J.; Odriozola, I.; Dupin, D. *Chem. Commun.* **2014**, *50*, 15199.
(18) de la Riva, H.; Pintado-Alba, A.; Nieuwenhuyzen, M.; Hardacre, C.; Lagunas, M. C. *Chem. Commun.* **2005**, 4970.
(19) Kim, P.-S. G.; Hu, Y.; Brandys, M.-C.; Burchell, T. J.; Puddephatt, R. J.; Sham, T. K. *Inorg. Chem.* **2007**, *46*, 949.
(20) Wedlock, L. E.; Aitken, J. B.; Berners-Price, S. J.; Barnard, P. J. *Dalton Trans.* **2013**, *42*, 1259.
(21) Deák, A.; Megyes, T.; Tárkányi, G.; Király, P.; Biczók, L.; Pálinkás, G.; Stang, P. J. *J. Am. Chem. Soc.* **2006**, *128*, 12668.

DOI: 10.1021/acs.inorgchem.5b00025
Inorg. Chem. 2015, 54, 5195−5203

(22) Tkatchouk, E.; Mankad, N. P.; Benitez, D.; Goddard, W. A.; Toste, F. D. *J. Am. Chem. Soc.* **2011**, *133*, 14293.
(23) Balzano, F.; Cuzzola, A.; Diversi, P.; Ghiotto, F.; Uccello-Barretta, G. *Eur. J. Inorg. Chem.* **2007**, *2007*, 5556.
(24) Horvath, U. E. I.; McKenzie, J. M.; Cronje, S.; Raubenheimer, H. G.; Barbour, L. J. *Chem. Commun.* **2009**, 6598.
(25) Gallego, M. L.; Guijarro, A.; Castillo, O.; Parella, T.; Mas-Balleste, R.; Zamora, F. *CrystEngComm* **2010**, *12*, 2332.
(26) Tárkányi, G.; Király, P.; Pálinkás, G.; Deák, A. *Magn. Reson. Chem.* **2007**, *45*, 917.
(27) Ferrer, M.; Gutiérrez, A.; Rodriguez, L.; Rossell, O.; Lima, J. C.; Font-Bardia, M.; Solans, X. *Eur. J. Inorg. Chem.* **2008**, *2008* (18), 2899.
(28) Elbjeirami, O.; Yockel, S.; Campana, C. F.; Wilson, A. K.; Omary, M. A. *Organometallics* **2007**, *26*, 2550.
(29) Elbjeirami, O.; Omary, M. A. *J. Am. Chem. Soc.* **2007**, *129*, 11384.
(30) Rawashdeh-Omary, M. A.; Omary, M. A.; Patterson, H. H. *J. Am. Chem. Soc.* **2000**, *122*, 10371.
(31) Jiang, X.-F.; Hau, F. K.-W.; Sun, Q.-F.; Yu, S.-Y.; Yam, V. W.-W. *J. Am. Chem. Soc.* **2014**, *136*, 10921.
(32) Yang, C.; Messerschmidt, M.; Coppens, P.; Omary, M. A. *Inorg. Chem.* **2006**, *45*, 6592.
(33) Rawashdeh-Omary, M. A.; Omary, M. A.; Patterson, H. H.; Fackler, J. P., Jr. *J. Am. Chem. Soc.* **2001**, *123*, 11237.
(34) Mayoral, M. J.; Ovejero, P.; Criado, R.; Lagunas, M. C.; Pintado-Alba, A.; Torres, M. R.; Cano, M. *J. Organomet. Chem.* **2011**, *696*, 2789.
(35) Rodríguez, L.; Ferrer, M.; Crehuet, R.; Anglada, J.; Lima, J. C. *Inorg. Chem.* **2012**, *51*, 7636.
(36) Gavara, R.; Llorca, J.; Lima, J. C.; Rodríguez, L. *Chem. Commun.* **2013**, *49*, 72.
(37) Aguiló, E.; Gavara, R.; Lima, J. C.; Llorca, J.; Rodríguez, L. *J. Mater. Chem. C* **2013**, *1*, 5538.
(38) Lanigan, N.; Wang, X. *Chem. Commun.* **2013**, *49*, 8133.
(39) García-Moreno, E.; Gascón, S.; Rodríguez-Yoldi, M. J.; Cerrada, E.; Laguna, M. *Organometallics* **2013**, *32*, 3710.
(40) Moro, A. J.; Rome, B.; Aguiló, E.; Arcau, J.; Puttreddy, R.; Rissanen, K.; Lima, J. C.; Rodríguez, L. *Org. Biomol. Chem.* **2015**, *13*, 2026.
(41) Smulders, M. M. J.; Nieuwenhuizen, M. M. L.; de Greef, T. F. A.; van der Schoot, P.; Schenning, A. P. H. J.; Meijer, E. W. *Chem.—Eur. J.* **2010**, 362.
(42) Ponnuswamy, N.; Pantoş, G. D.; Smulders, M. M. J.; Sanders, J. K. M. *J. Am. Chem. Soc.* **2012**, *134*, 566.
(43) Tambara, K.; Olsen, J.-C.; Hansen, D. E.; Dan Pantos, G. *Org. Biomol. Chem.* **2014**, *12*, 607.
(44) te Velde, G.; Bickelhaupt, F. M.; van Gisbergen, S. J. A.; Fonseca Guerra, C.; Baerends, E. J.; Snijders, J. G.; Ziegler, T. *J. Comput. Chem.* **2001**, *22*, 931.
(45) *ADF2013*; SCM: Theoretical Chemistry, Vrije Universiteit, Amsterdam, The Netherlands, http://www.scm.com (accessed May 1, 2015).
(46) Pyykkö, P. *Angew. Chem., Int. Ed.* **2004**, *43*, 4412.
(47) Fonseca Guerra, C.; Bickelhaupt, F. M.; Snijders, J. G.; Baerends, E. J. *Chem.—Eur. J.* **1999**, *5*, 3581.
(48) Fonseca Guerra, C.; Bickelhaupt, F. M.; Baerends, E. J. *ChemPhysChem* **2004**, *5*, 481.
(49) Grimme, S.; Ehrlich, S.; Goerigk, L. *J. Comput. Chem.* **2011**, *32*, 1456.
(50) van Lenthe, E.; Baerends, E. J.; Snijders, J. G. *J. Chem. Phys.* **1994**, *101*, 9783.
(51) Schreckenbach, G.; Ziegler, T. *J. Phys. Chem.* **1995**, *99*, 606.
(52) Klamt, A.; Schüürmann, G. *J. Chem. Soc., Perkin Trans.* **1993**, *2*, 799.
(53) Klamt, A. *J. Phys. Chem.* **1995**, *99*, 2224.
(54) Pye, C. C.; Ziegler, T. *Theor. Chem. Acc.* **1999**, *101*, 396.
(55) Swart, M.; Rösler, E.; Bickelhaupt, F. M. *Eur. J. Inorg. Chem.* **2007**, *2007*, 3646.

DOI: 10.1021/acs.inorgchem.5b00025
Inorg. Chem. 2015, 54, 5195−5203